Biophysical Letter

Real-Time Imaging of Electrical Signals with an Infrared FDA-Approved Dye

Jeremy S. Treger,[1] Michael F. Priest,[1,2] Raymond Iezzi,[3] and Francisco Bezanilla[1,2,*]
[1]Department of Biochemistry and Molecular Biology and [2]Committee on Neurobiology, University of Chicago, Chicago, Illinois; and [3]Department of Ophthalmology, Mayo Clinic, Rochester, Minnesota

ABSTRACT Clinical methods used to assess the electrical activity of excitable cells are often limited by their poor spatial resolution or their invasiveness. One promising solution to this problem is to optically measure membrane potential using a voltage-sensitive dye, but thus far, none of these dyes have been available for human use. Here we report that indocyanine green (ICG), an infrared fluorescent dye with FDA approval as an intravenously administered contrast agent, is voltage-sensitive. The fluorescence of ICG can follow action potentials in artificial neurons and cultured rat neurons and cardiomyocytes. ICG also visualized electrical activity induced in living explants of rat brain. In humans, ICG labels excitable cells and is routinely visualized transdermally with high spatial resolution. As an infrared voltage-sensitive dye with a low toxicity profile that can be readily imaged in deep tissues, ICG may have significant utility for clinical and basic research applications previously intractable for potentiometric dyes.

Received for publication 23 June 2014 and in final form 30 July 2014.

*Correspondence: fbezanilla@uchicago.edu

Jeremy S. Treger and Michael F. Priest contributed equally to this article.

Voltage-sensitive dyes provide a way to observe cellular electrical activity without the physical limitations imposed by electrodes. Although these dyes can monitor membrane potential with a resolution of a few microns from large populations of cells (1), there are three obstacles that prevent the use of these dyes in many research settings, including clinical research:

1. Most voltage-sensitive dyes use visible wavelengths of light that prevent imaging of tissues beneath the skin.
2. Many of these dyes produce significant toxicity or off-target effects (2).
3. Before this report, to our knowledge, no voltage-sensitive dyes have ever been available for administration in humans, which has limited their value in biomedically focused research.

Here, we show that indocyanine green (ICG), an FDA-approved fluorescent dye routinely used in many clinical tests, is voltage-sensitive. Our initial experimental system used *Xenopus laevis* oocytes. Changes in the membrane potential of the cell induced by two-electrode voltage-clamp resulted in robust, consistent changes in the fluorescence of ICG (Fig. 1, *inset*). All data in this work was obtained from single acquisitions with no averaging of multiple images. The voltage-dependent fluorescence changes were roughly linear with respect to membrane potential and had a magnitude of ~1.9% of the baseline fluorescence per 100 mV of membrane potential change (Fig. 1). Additionally, ICG displayed a rapid response with a primary time constant of 4 ms (see Fig. S1 in the Supporting Material), suggesting that this dye could successfully monitor action potentials.

To test this hypothesis, we transformed our oocytes into synthetic neurons, previously dubbed "excitocytes", by coinjecting them with cRNA of voltage-gated sodium (Na_v) and potassium channel components (3). Under suitable current-clamp conditions, excitocytes fire trains of action potentials similar to those in naturally excitable cells. ICG's fluorescence clearly recapitulated action potentials firing at speeds above 100 Hz (Fig. 2 *A*), faster than the physiological firing rates of most neurons (4).

We extended the excitocyte technique from wild-type channels to evaluation of channelopathies and their effects on excitability to determine whether ICG could discriminate between normal and diseased action potentials based on shape. We compared excitocytes injected with wild-type Na_v channel cRNA to those injected with cRNA coding for a version of Na_v channel containing a point mutation, G1306E, which produces episodic myotonia (5). This disease is characterized by continued action potential firing in skeletal muscles after cessation of voluntary stimuli;

Editor: Brian Salzberg.

http://dx.doi.org/10.1016/j.bpj.2014.07.054

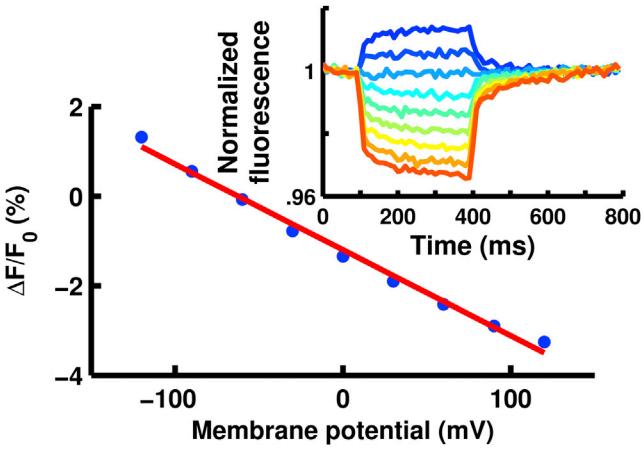

FIGURE 1 ICG-labeled oocytes showed that ICG's fluorescence (*blue points*) is roughly linearly dependent (*red line*, fit to data) with voltage. (*Inset*) Oocyte membrane potential was held at −60 mV and then pulsed to potentials ranging from −120 mV (*blue*) to +120 mV (*red*). Ex: 780 nm, Em: 818–873 nm.

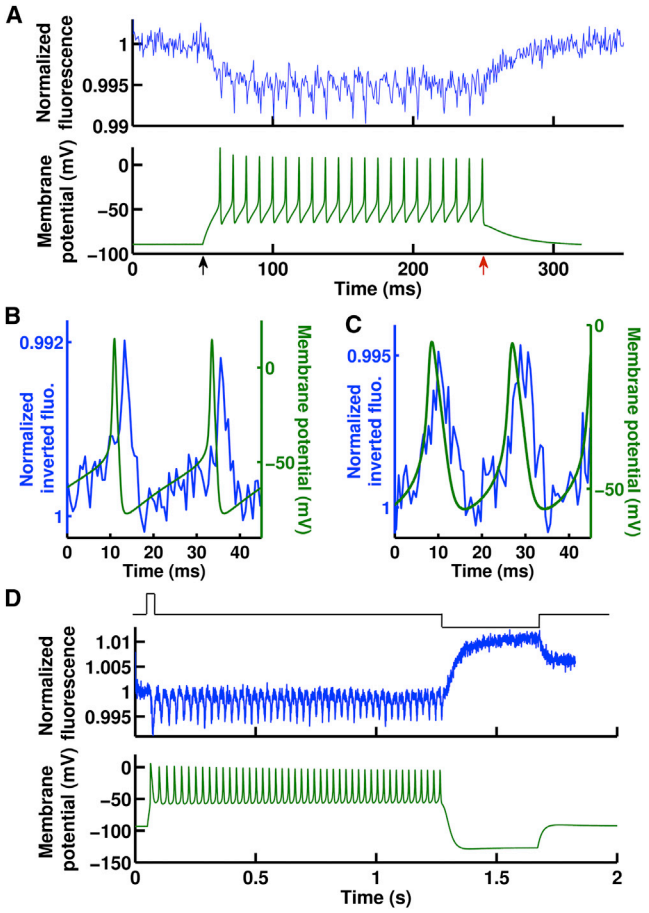

FIGURE 2 ICG can monitor action potentials. (*A*) Oocytes coinjected with voltage-gated sodium and potassium channel cRNA fired action potentials (*bottom, green*) when held under current clamp. ICG fluorescence changes (*top*, *blue*) detected these action potentials at a rate of 107 Hz. Stimulus start (*black arrow*) and end (*red arrow*) are shown. (*B* and *C*) ICG fluorescence (*blue*, inverted) distinguished between healthy action potentials from wild-type sodium channels (*B*, *green*) and diseased action potentials from sodium channels with a myotonic substitution (*C*, *green*). Cells are stimulated for the entire time course of these panels. The delay between action potentials and the ICG signal is due to a low-pass filtering effect caused by the dye response time and the camera integration time. (*D*) In cells with myotonic sodium channels, a brief stimulus (*top*, *black*) was sufficient to elicit a train of action potentials (*bottom*, *green*) that only ceased upon significant hyperpolarization, as expected in a myotonia. ICG fluorescence (*middle*, *blue*) successfully followed each one of these action potentials.

the resulting prolonged muscle contractions are the hallmark of myotonia. Compared to the wild-type Na_v channel, the G1306E mutation causes a slowing of the fast inactivation of the Na_v channels, which in turn results in broadened action potentials (5). The electrical recordings and the ICG fluorescence response clearly distinguished the sharp action potentials produced by the healthy sodium channel (Fig. 2 *B*, and see Fig. S2) from the wider peaks produced by the myotonic sodium channel (Fig. 2 *C*, and see Fig. S2). Furthermore, a brief injection of current led to repetitive firing and hyperexcitability that persisted after the stimulus was stopped. ICG fluorescence clearly resolved every action potential of this myotonia-like behavior (Fig. 2 *D*). The successful recreation of disease-like action potentials validates the excitocyte system as a convenient method for investigating the electrophysiological effects of channelopathies.

We next investigated whether ICG's voltage sensitivity extended to excitable mammalian tissue. This validation was critical, inasmuch as other voltage-sensitive dyes have shown promise in invertebrate preparations but had much smaller signals in mammalian cells (6). We first measured ICG fluorescence from cultured rat dorsal root ganglion neurons. Under whole-cell current clamp, we observed neurons firing in the stereotypical fashion of the nociceptive C-type fiber, and these action potentials were clearly visible in the ICG fluorescence (Fig. 3 *A*, and see Fig. S3). We also examined syncytia of cultured cardiomyocytes from neonatal rats (7) to further validate ICG's utility; these cells beat spontaneously and showed changes in ICG fluorescence indicative of changes in membrane potential (Fig. 3 *B*). Although we cannot formally exclude the possibility that the cardiomyocytes' physical motion produced fluorescence changes, several observations suggested that these effects were minimal (see Fig. S4). Taken together, our results in frog and rat cells confirmed that ICG voltage sensitivity was broadly applicable across a range of tissues and not confined to a particular animal or cell lineage.

Finally, we tested whether ICG voltage sensitivity could be detected in a complex tissue. Rat hippocampal slice cultures comprise a well-described organotypic preparation in which the three-dimensional architecture, neuronal connections, and glial interactions are maintained (8,9). Using these rat brain explants, we found that brain excitation

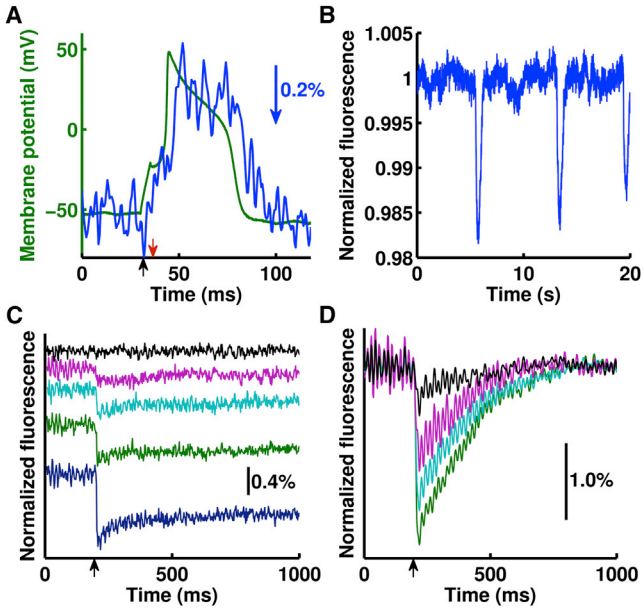

FIGURE 3 ICG follows electrical activity in living mammalian tissue. (*A*) Rat cultured dorsal root ganglion cells under current-clamp (*black arrow*, pulse start; *red arrow*, pulse end) fired action potentials (*green*), that ICG fluorescence tracked (*blue*, inverted, low-pass-filtered at 225 Hz; *blue arrow*, relative fluorescence change). (*B*) ICG fluorescence sensed spontaneous membrane potential changes in cardiomyocyte syncytia. (*C*) In rat brain slices, ICG responds differently to no stimulus (*black*) and stimuli of increasing intensity (*magenta*, *cyan*, *green*, and *blue*, increasing amplitude; scale bar shows relative fluorescence change). Weaker stimuli traces (e.g., *magenta*) show complete fluorescence recovery whereas larger stimuli (e.g., *blue*) do not fully recover within this time course; traces are vertically offset for clarity. (*D*) Tetrodotoxin (TTX) reduced the ICG response to a stimulus over 12 min (*green*, pre-TTX; *cyan*, *magenta*, and *black*, increasing time post-TTX; low-pass-filtered at 40 Hz; *black arrow*, stimulus).

produced by field electrode stimulation was clearly accompanied by ICG fluorescence changes (see Fig. S5). Additionally, ICG discriminated between electrical responses caused by differing excitation intensities and durations (Fig. 3 *C*, and see Fig. S5). To confirm that the fluorescence changes originated from changes in excitable cell activity, we used the Na_v channel blocker tetrodotoxin (TTX). When applied to brain slices, electrical excitability was clearly inhibited (Fig. 3 *D*, and see Fig. S5) and partial recovery was observed upon subsequent TTX removal (see Fig. S5). These signals measuring brain slice activity were similar in shape and magnitude to those reported using other voltage-sensitive dyes (10,11). This demonstrates that ICG can report on electrical activity even in a physiological architecture with many nonexcitable cells.

To our knowledge, this is the first report that a clinically approved fluorescent dye is voltage-sensitive. Our results demonstrate that indocyanine green can accurately detect action potentials at firing rates common in mammalian neurons, and that it is sensitive enough to distinguish between healthy and diseased action potentials in a model system. ICG can measure electrical activity in mammalian neurons, cardiomyocytes, and explanted brain tissue. This voltage sensitivity was observed with both monochromatic and broad-band illumination sources (data not shown), under labeling conditions that differed in solution composition, duration, and dye concentration (see Methods in the Supporting Material), and at temperatures ranging from 19°C to 30°C. ICG's water solubility further extends its potential utility. This robustness suggests that ICG can be used to measure voltage in many environments and tissues.

ICG has been FDA-approved for use in ophthalmic angiography, as well as in tests of cardiac output and hepatic function (12) and is additionally used off-label in a number of surgical applications (13). Interestingly, ICG has been shown to clearly label retinal ganglion cells in human patients (see Fig. S6) (14). This provides immediate motivation for biomedical investigations, because laboratory findings with ICG can potentially be translated to humans. Although many other voltage-sensitive dyes have been described, some with similar structures to ICG (15) and others with faster or larger signals (15,16), as of this writing none of these are FDA-approved. Additionally, ICG utilizes wavelengths further into the infrared spectrum than other available fast potentiometric dyes (17) and can thus be imaged in tissues up to 2 cm deep (18). This presents the possibility of optically imaging electrical activity deeper inside tissues than is feasible today. Although two-photon excitation with voltage-sensitive dyes can improve imaging depth, it remains intrinsically limited by the unaffected emission wavelength (19). Finally, ICG has been used in patients for more than 50 years and is known to have low toxicity (18,20). These properties suggest that ICG voltage sensitivity could extend the capabilities of modern electrophysiological techniques for disease diagnosis and monitoring in the clinic, and allow for the investigation of previously inaccessible experimental systems in basic research.

SUPPORTING MATERIAL

Six figures, supporting methods, and data analysis are available at http://www.biophysj.org/biophysj/supplemental/S0006-3495(14)00801-7.

ACKNOWLEDGEMENTS

We thank Aya Pusic, Lisa Won, and Dr. Richard Kraig for brain slices and cardiomyocyte culture rats, Dr. Maria Traka for neuron culture rats, and Dr. Joao de Souza for patch-clamp assistance.

Support was provided by NIH grant GM030376. NIH GM07281 provided extra support to J.S.T, NS081954 to M.F.P and the Mayo Foundation for Medical Research and Research to Prevent Blindness to R.I.

SUPPORTING CITATIONS

Ref. (21) appears in the Supporting Material.

REFERENCES and FOOTNOTES

1. Cohen, L. B., and B. M. Salzberg. 1978. Optical measurement of membrane potential. *Rev. Physiol. Biochem. Pharmacol.* 83:35–88.
2. Peterka, D. S., H. Takahashi, and R. Yuste. 2011. Imaging voltage in neurons. *Neuron.* 69:9–21.
3. Shapiro, M. G., M. F. Priest, …, F. Bezanilla. 2013. Thermal mechanisms of millimeter wave stimulation of excitable cells. *Biophys. J.* 104:2622–2628.
4. Buzsáki, G., and K. Mizuseki. 2014. The log-dynamic brain: how skewed distributions affect network operations. *Nat. Rev. Neurosci.* 15:264–278.
5. Lerche, H., R. Heine, …, F. Lehmann-Horn. 1993. Human sodium channel myotonia: slowed channel inactivation due to substitutions for a glycine within the III-IV linker. *J. Physiol.* 470:13–22.
6. Ross, W. N., and L. F. Reichardt. 1979. Species-specific effects on the optical signals of voltage-sensitive dyes. *J. Membr. Biol.* 48:343–356.
7. Fu, J., J. Gao, …, P. Liu. 2005. An optimized protocol for culture of cardiomyocyte from neonatal rat. *Cytotechnology.* 49:109–116.
8. Pusic, A. D., K. M. Pusic, …, R. P. Kraig. 2014. IFNγ-stimulated dendritic cell exosomes as a potential therapeutic for remyelination. *J. Neuroimmunol.* 266:12–23.
9. Pusic, A. D., Y. Y. Grinberg, …, R. P. Kraig. 2011. Modeling neural immune signaling of episodic and chronic migraine using spreading depression in vitro. *J. Vis. Exp.* 52:2910. http://dx.doi.org/10.3791/2910.
10. Carlson, G. C., and D. A. Coulter. 2008. In vitro functional imaging in brain slices using fast voltage-sensitive dye imaging combined with whole-cell patch recording. *Nat. Protoc.* 3:249–255.
11. Contreras, D., and R. Llinas. 2001. Voltage-sensitive dye imaging of neocortical spatiotemporal dynamics to afferent activation frequency. *J. Neurosci.* 21:9403–9413.
12. Akorn, Inc. 2012. IC-GREEN [package insert]. Akorn, Lake Forest, IL.
13. Alander, J. T., I. Kaartinen, …, P. Välisuo. 2012. A review of indocyanine green fluorescent imaging in surgery. *Int. J. Biomed. Imaging.* 2012:940585.
14. Ashikari, M., H. Ozeki, …, Y. Ogura. 2006. Long-term retention of dye after indocyanine green-assisted internal limiting membrane peeling. *Jpn. J. Ophthalmol.* 50:349–353.
15. Cohen, L. B., B. M. Salzberg, …, C. H. Wang. 1974. Changes in axon fluorescence during activity: molecular probes of membrane potential. *J. Membr. Biol.* 19:1–36.
16. Loew, L. M. 2011. Design and use of organic voltage sensitive dyes. *In* Membrane potential imaging in the nervous system: methods and applications. M. Canepari and D. Zecevic, editors. Springer, New York, pp. 13–23.
17. Matiukas, A., B. G. Mitrea, …, L. M. Loew. 2006. New near-infrared optical probes of cardiac electrical activity. *Am. J. Physiol. Heart Circ. Physiol.* 290:H2633–H2643.
18. Marshall, M. V., J. C. Rasmussen, …, E. M. Sevick-Muraca. 2010. Near-infrared fluorescence imaging in humans with indocyanine green: a review and update. *Open Surg. Oncol. J.* 2:12–25.
19. Fisher, J. A. N., J. R. Barchi, …, B. M. Salzberg. 2008. Two-photon excitation of potentiometric probes enables optical recording of action potentials from mammalian nerve terminals in situ. *J. Neurophysiol.* 99:1545–1553.
20. Frangioni, J. V. 2003. In vivo near-infrared fluorescence imaging. *Curr. Opin. Chem. Biol.* 7:626–634.
21. Narahashi, T., J. W. Moore, and W. R. Scott. 1964. Tetrodotoxin blockage of sodium conductance increase in lobster giant axons. *J. Gen. Physiol.* 47:965–974.

Real-time imaging of electrical signals with an infrared FDA-approved dye

Supporting Information

Jeremy S. Treger,* ¶ Michael F. Priest,† ¶ Raymond Iezzi,‡ and Francisco Bezanilla*†

*Department of Biochemistry and Molecular Biology, University of Chicago, Chicago, IL;
†Committee on Neurobiology, University of Chicago, Chicago, IL;
‡Department of Ophthalmology, Mayo Clinic, Rochester, MN;
¶These authors contributed equally

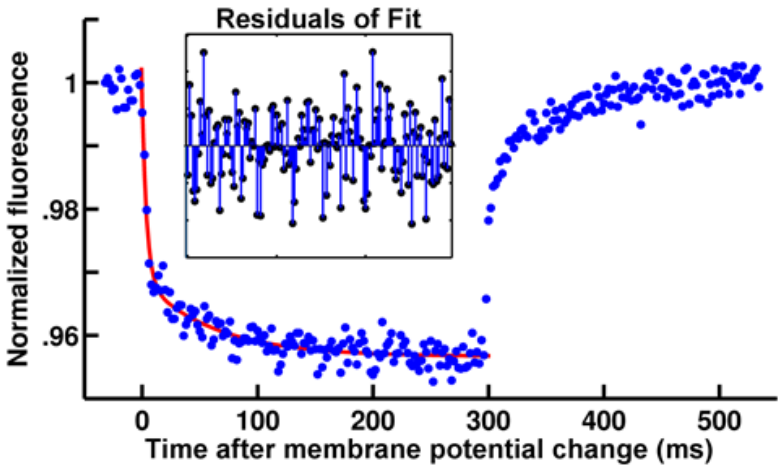

Figure S1: Kinetics of the indocyanine green voltage-sensitive response. The kinetics of the change in fluorescence of ICG in response to a change in membrane potential (*blue*) can be fit by a double exponential function (*red line*, see inset for residuals). The time constant of the faster component, which comprises the majority of the fluorescence change, was 4.0 ms, while the time constant of the slower component was 62 ms. During this recording the time constant of the voltage-clamp was 150 μs; the camera was running at a 500 Hz frame rate.

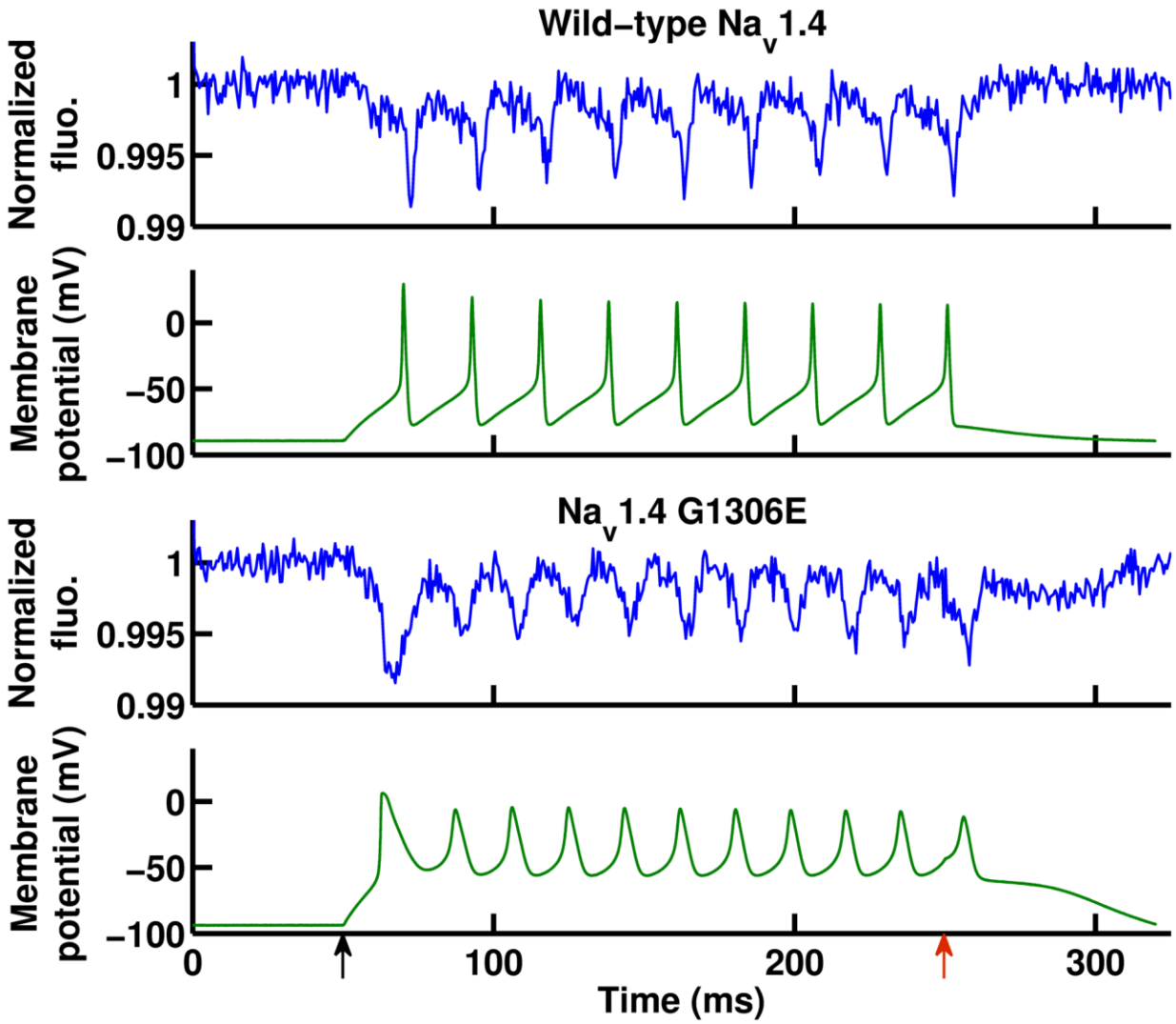

Figure S2: ICG follows the shapes of action potentials. ICG fluorescence (*blue*, upper rows of each construct) follows action potentials (*green*, lower rows) fired by excitocytes in response to an injection of current (beginning at black arrow and ending at red arrow). The fluorescence follows the shape of the action potentials, discriminating between action potentials generated by wild-type $Na_v1.4$ (top pair, full time course of Fig. 2 *B*) and action potentials generated by mutant $Na_v1.4$ with the G1306E myotonia substitution (bottom pair, full time course of Fig. 2 *C*).

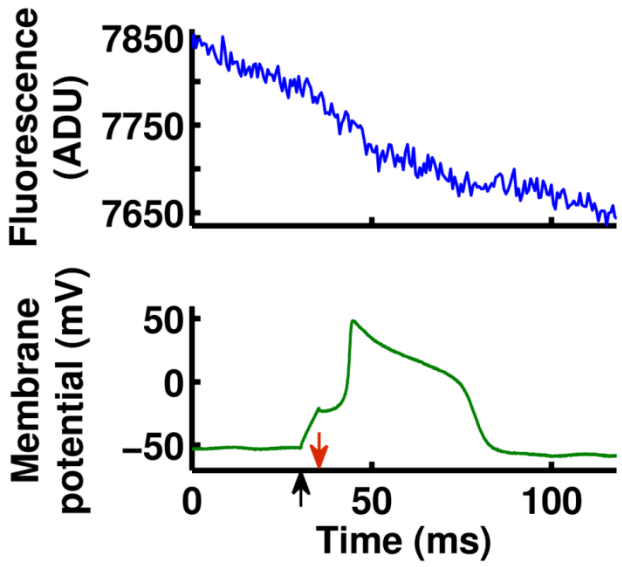

Figure S3: Unprocessed data from cultured rat neurons demonstrates voltage sensitivity. Unprocessed data of ICG fluorescence from Fig. 3 *A* in the main text (*top, blue*). This is an average of all pixels in the field of view, including those outside of the neuron, causing the reduction in signal to noise. Additionally, no bleach correction or filtering has been applied. An injection of depolarizing current was given from the black arrow until the red arrow, resulting in an action potential (*bottom, green*, identical to Fig. 3 *A*).

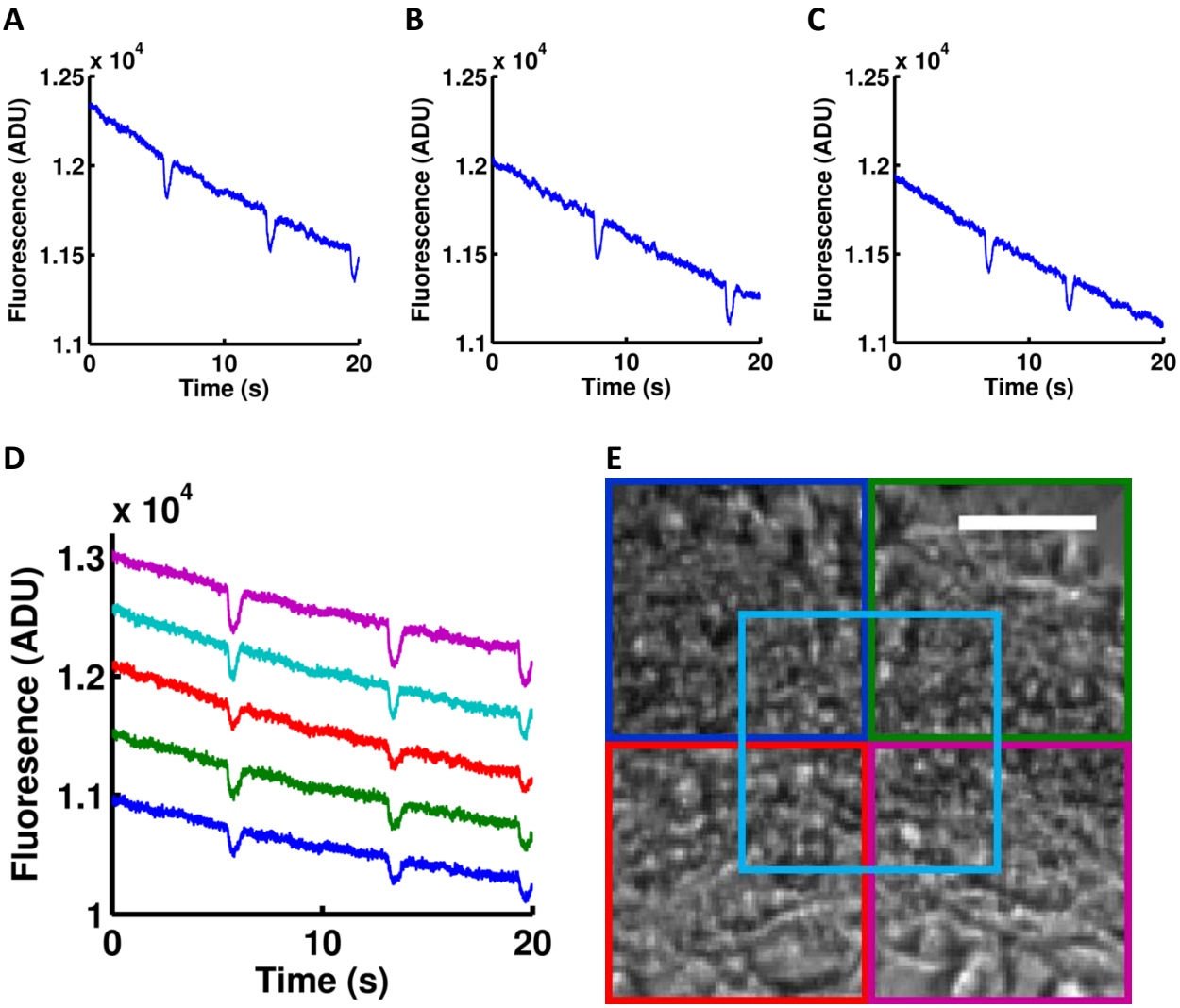

Figure S4: Fluorescence changes in cardiomyocyte syncytia are not due to contractile movement. (*A*, *B*, *C*) Motion in the z-axis that takes the syncytium out of the microscope's focal plane would result in fluorescence signals similar to what we see in (*A*), the unprocessed ICG fluorescence from a cardiomyocyte syncytium (same data as Fig. 3 *B* in the main text). However, intentionally focusing the microscope above (*B*) or below (*C*) the syncytium should produce the opposite effect, as the syncytium would move into the new focal plane, increasing fluorescence during each contraction. Instead, all focal planes display similar behavior, suggesting that no prominent z-axis motions are responsible for observed ICG fluorescence changes. (*D*, *E*) Similarly, motion in the x-y plane could decrease fluorescence by removing bright areas or bringing dim areas into the field of view. In this case, different parts of the field of view should have drastically different signals with some regions displaying net increases in fluorescence by chance. Instead, we observe in (*D*) a systematic decrease in fluorescence in each individual syncytial quadrant; the quadrants are mapped in (*E*): left-upper, blue; right-upper, green; right-lower, magenta; left-lower, red; center; cyan. In all panels, ADU stands for analog-to-digital units, the camera output. The scale bar is 40 μm.

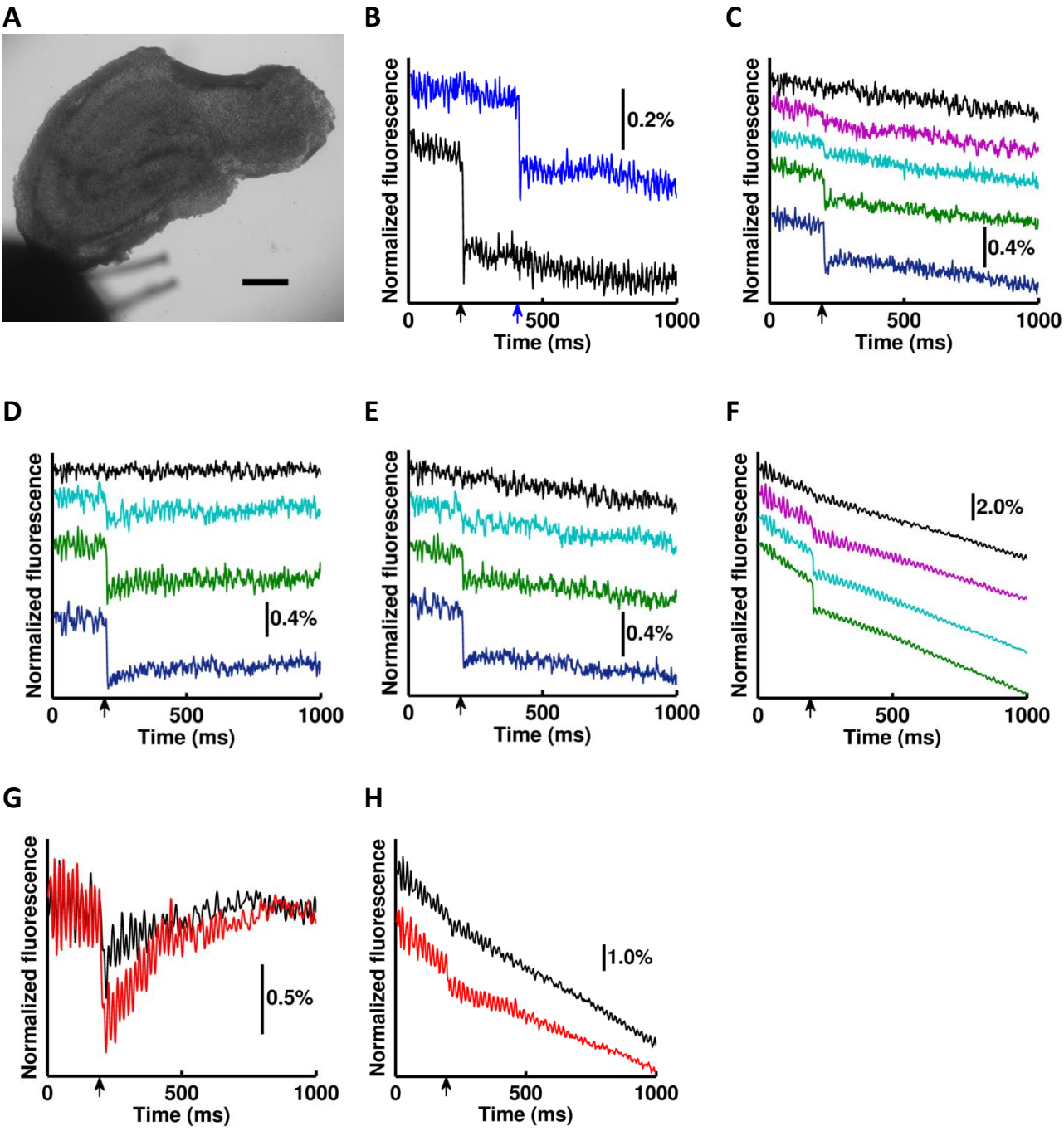

Figure S5: Hippocampal slices show clear ICG fluorescence changes as a result of electrical activity. (*A*) Cultured hippocampal brain slices from neonatal rats maintain glial cells and the three-dimensional structure of the hippocampus. In the lower left of the image, the bipolar stimulating microelectrodes can be seen. The scale bar is 0.5 mm. (*B*) Unprocessed data of slice stimulations at 200 ms (*bottom trace*, *black*) and 400 ms (*top trace*, *blue*) after recording. Changing the timing of the stimulus pulse (*black* and *blue* arrows for the bottom and top traces, respectively) changes the timing of the ICG fluorescence change. For this and subsequent panels, traces are offset vertically for clarity and the scale bar shows the size of a given relative fluorescence change. (*C*) As in Fig. 3 *C*, with stimuli of varying

intensities (*black* – no pulse; *magenta*, *cyan*, *green*, and *blue*, in order of increasing stimulus amplitude), but data is unprocessed. All unprocessed data in this figure is an average of all pixels in the image and has no filtering or bleach correction. (*D*) Similar to *C*, but the duration of the stimulus pulse is varied rather than the intensity (*black* – no pulse; *cyan* – short; *green* – intermediate; *blue* – long). (*E*) As in *D*, but unprocessed data. (*F*) Fig. 3 *D* of gradual tetrodotoxin (TTX) block (*green* – before TTX; *cyan*, *magenta*, *black* – increasing time after TTX), shown here without processing. (*G*) Following washout of TTX, excitability and ICG response were partially recovered (*black* – before washout, same as *black* in Fig. 3 *D*; *red* – 5 minutes after washout). Partial recovery is unsurprising as completely removing TTX block is often impractical (1). (*H*) The data shown in *G* without processing. As the unprocessed traces (*B*, *C*, *E*, *F*, and *H*) demonstrate, potential artifacts that could arise from our data processing are not responsible for the observed changes in ICG fluorescence.

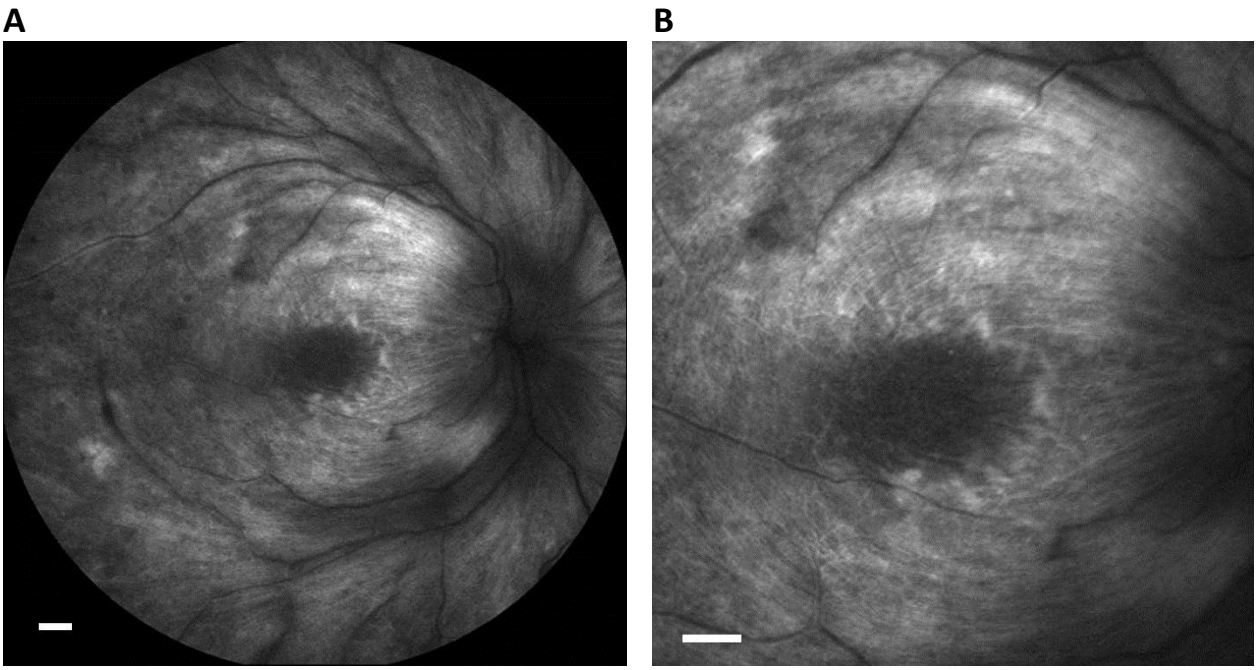

Figure S6: ICG labels retinal ganglion cells (RGCs) in patients after a common ophthalmological procedure. (*A*) ICG intraoperatively applied to the retina of a patient with retinitis pigmentosa clearly stained RGC axons when observed with a scanning laser ophthalmoscope on post-operative day 1. Blood vessels (dark branching structures) converging at the optic disc (dark circular region on far right) show little to no ICG fluorescence due to the rapid rate of ICG clearance from blood. The dark region in the center of the image is the macula with its much lower RGC density. Strong ICG fluorescence (seen in *white)* is clearly seen in numerous RGCs running parallel to each other as they arc from the macula to the optic disc to form the optic nerve, as expected. The scale bar is 800 μm. Observation of ICG voltage dependence in human patients has not yet been attempted. (*B*) A higher magnification image of the same retina, more clearly showing RGC fibers running from the macula (center of image) to the optic disc (right border of image). The scale bar is 800 μm.

Methods

Optical Equipment

ICG fluorescence was monitored using an Evolve 128 EMCCD camera (Photometrics, Tucson, Arizona) attached to an Olympus IX71 inverted microscope (Center Valley, Pennsylvania). The camera CCD is 128x128 pixels and can acquire images at up to 500 Hz full-frame. Binning pixels allowed us to acquire images at 1.8 kHz for preparations in which high spatial resolution was unnecessary, such as oocytes and individual neurons. The dye was excited with a 780 nm diode laser (World Star Technologies, Toronto, Canada), and the Indocyanine Green filter set from Chroma Technology Corp. (49030 ET, Bellows Falls, Vermont) was used to isolate fluorescence emission. Various microscope objectives were used for different preps ranging from a 20X/0.45NA air lens to a 60X/1.45NA oil immersion lens. Raw excitation power varied widely depending on the objective lens in use, but illumination intensity was typically about 0.5 W/cm^2. Retinal imaging was performed using a scanning laser ophthalmoscope (HRA-2, Heidelberg Engineering, Heidelberg, Germany). Excitation of ICG was performed at 795 nm and emission was imaged at wavelengths longer than 810 nm using a 30 degree field of view.

Electrophysiological Equipment

Two-electrode voltage clamp was performed with a Warner Instruments OC-725A amplifier (Hamden, Connecticut). For current clamp, a 100 MΩ resistance was placed in series with the oocyte. Micropipettes were pulled to approximately 0.5 MΩ on a Flaming/Brown micropipette puller (Sutter Instruments, Novata, California, model P-87) and filled with 3 M KCl. Stimulation of rat brain tissue was accomplished via a homemade platinum bipolar field electrode. Patch-clamp of cultured cells was performed using a Dagan 3900 integrating patch clamp amplifier (Minneapolis, Minnesota). Patch pipettes were pulled to approximately 5 MΩ on a CO_2 laser micropipette puller (Sutter Instruments, model P-2000), fire polished immediately prior to use, and filled with patch pipette solution (see Materials and Solutions below). Amplifier outputs were filtered through an 8-pole low-pass Bessel filter (Frequency Devices, Ottawa, Illinois, model 950L8L) and digitized with an SBC-6711-A4D4 data acquisition board (Innovative Integration, Simi Valley, CA). Filter cutoff frequency was set to approximately one fourth of the digitizing sample frequency. The acquisition board was also used to control the clamp and synchronize optical and electrical acquisitions. Software programs for both electrical control and camera control were written in-house.

Tissue preparation protocols

Oocytes were digested in OR2 with collagenase and bovine serum albumin added and incubated in SOS. Excitocytes were prepared by coinjecting cRNAs of Nav1.4 α and β subunits with cRNA of a clone of the Shaker Kv channel with fast inactivation removed as described previously (2) and waiting 2-4 days for channels to express sufficiently. Uninjected oocytes were labeled in 0.0155 mg/ml (20 μM) ICG in SOS for 5-15 minutes. Labeled oocytes were then rinsed and recorded in SOS. Labeling and recording protocols for excitocytes were identical to those for uninjected oocytes apart from the recording solution which had reduced calcium in excitocyte recordings. Oocyte recordings were performed at

room temperature of around 19 °C. Excitocyte recordings were performed at room temperature of around 19 °C, except for tests of high frequency firing, which were performed in a bath at around 30 °C.

Dorsal root ganglia were harvested from spinal cords taken from P2-P6 Sprague-Dawley rats and digested to isolate individual neurons. These cells were then cultured in DMEM (supplemented with 10% fetal bovine serum and 100 U/ml of penicillin and 100 μg/ml of streptomycin) for 24 hours prior to recording. Immediately prior to use, cells were rinsed in patch bath solution, labeled in 0.00775 mg/ml (10 μM) ICG for one to two minutes and rinsed in patch bath solution again for recording. Neuron recordings were performed at room temperature.

Cardiomyocytes were cultured from hearts harvested from P1 neonatal Wistar rats. Hearts were digested in EBSS with 0.08% trypsin similar to prior descriptions (3). Modifications to the protocol included shaking in an incubator rather than on a magnetic stirrer and substituting EBSS with fetal bovine serum for cold culture media with a trypsin inhibitor. Cells were plated on glass coverslips coated in fibronectin. Cardiomyocytes were incubated in DMEM with 10% fetal bovine serum and 100 U/ml of penicillin and 100 μg/ml of streptomycin added. Cardiomyocytes were labeled in 0.00155 mg/ml (2 μM) ICG in DMEM for 1-10 minutes. Cardiomyocyte recordings were performed at 24 °C.

Hippocampal cultured brain slices were prepared as described previously (4, 5). During labeling and prior to recording, slices were kept in a humidified carbogen (95% O_2 / 5% CO_2) atmosphere in a pipette tip box, similar to prior descriptions (6). Slices were labeled in .031 mg/ml (40 μM) ICG in GBSS for 15-20 minutes. Slices were subsequently rinsed in GBSS and recorded in fresh GBSS. Tetrodotoxin stock was diluted to 1 μM in GBSS immediately before use. After application, it was washed out with fresh GBSS. All brain slice solutions were bubbled with carbogen prior to use. Brain slice recordings were performed at room temperature; activity was stimulated with a field electrode using symmetric bipolar pulses to prevent electrode polarization. The maximum stimulus duration was 6 ms in total (a 3 ms pulse in one polarity immediately followed by a 3 ms pulse in the opposite polarity).

All tissue harvesting was performed in accordance with protocols approved by the University of Chicago Animal Care and Use Committee.

For the retinal images, a 0.08 mg/ml ICG in a 5% dextrose solution was directly applied to the retina of a patient with retinitis pigmentosa to aid in peeling the epiretinal membrane during a surgical procedure. The patient's retina was imaged one day after this procedure.

Materials and Solutions

Indocyanine green was obtained in both the clinical formulation as IC-Green (Akorn, Lake Forest, Illinois) and non-clinical formulation as Cardiogreen (Sigma-Aldrich, St. Louis, Missouri). No appreciable differences were found between the two sources. Dye was dissolved in DMSO at a concentration of 20 mM and stored in aliquots at -80 °C. Immediately prior to use, aliquots were thawed and sonicated briefly.

Antibiotics and other salt solution additives: Streptomycin (Sigma-Aldrich), penicillin (Sigma-Aldrich), gentamicin (Sigma-Aldrich), trypsin-TRL3 (Worthington, Lakewood, New Jersey), fetal bovine serum (ATCC, Manassas, Virginia), and DNaseI (Sigma-Aldrich)

Tetrodotoxin (Abcam, Cambridge, United Kingdom) was stored in a 3 mM stock solution in water.

Concentrations are in mM unless otherwise stated

OR2: 82.5 NaCl, 2.5 KCl, 2 $MgCl_2$, 10 HEPES, pH 7.4

Standard oocyte solution (SOS): 96 NaCl, 2 KCl, 1 $MgCl_2$, 1.8 $CaCl_2$, 10 HEPES, pH 7.4, 50 μg/ml of gentamicin

Excitocyte recording solution: Same as SOS but with 0.6 $CaCl_2$ and no gentamicin

EBSS: 132 NaCl, 5.3 KCl, 1 NaH_2PO_4, 10 HEPES, 5.5 glucose, pH 7.4

DMEM: HyClone-DMEM/High Glucose with high glucose, L-glutamine, sodium pyruvate, and phenol red (LifeTechnologies, Carlsbad, California, currently GELifeSciences, Piscataway, New Jersey)

Patch bath solution: 132 NaCl, 6 KCl, 1.8 $CaCl_2$, 1.2 $MgCl_2$, 10 HEPES, 5 glucose, pH 7.4

Patch pipette solution: 150 KF, 10 NaCl, 4.5 $MgCl_2$, 2 ATP, 9 EGTA, 10 HEPES, pH 7.4, filtered

GBSS (Sigma) or made with 137 NaCl, 5 KCl, 1.5 $CaCl_2$, 1 $MgCl_2$, 2.7 $NaHCO_3$, 0.22 KH_2PO_4, 0.28 $MgSO_4$, 0.85 Na_2HPO_4, 5.6 glucose, pH 7.4

Data Analysis

Movies were converted into time-dependent traces by averaging pixel values for each frame of a given movie. Images of oocyte membranes and cardiomyocyte syncytia showed relatively little variation in signal size across different regions of the field of view, so all pixels of each frame were used. Dorsal root ganglion neurons, in contrast, occupied only about 30% of the field of view, so a level threshold was used to isolate neuronal pixels from the non-fluorescent background. Finally, the hippocampal slices contained regions that were largely quiescent. Although the voltage-dependent signal was clearly visible when averaging all pixels, the signal-to-noise ratio was greatly improved by selecting only regions of the image that displayed the most voltage sensitivity. These regions were located by first identifying the single pixels which contained the largest signal and then using morphological image processing to create a binary mask for the image. Morphological operations were based on a diamond-shaped structuring element and utilized repeated openings and closings. Although the exact parameters used were arbitrarily chosen, the resulting signal was qualitatively insensitive to exact choices of morphological parameters. The net effect of these operations was to delineate regions enriched in active pixels and reject the remainder of the image. Once a mask was defined for an image, it was applied to all frames in the movie so that the same pixels would be averaged in each frame to create the time-dependent trace. All traces shown in this work are derived from single acquisitions with no averaging of separate movies.

Once movies had been converted into time-dependent traces by averaging some or all pixels in each frame, the traces were corrected for photobleaching. This was achieved by fitting an exponential curve to all parts of the trace which did not exhibit a voltage-dependent signal and then subtracting this fitted curve from the original trace. In most cases a single exponential function was sufficient to provide a good fit of bleaching. Fluorescence traces from dorsal root ganglion neurons and hippocampal slices were digitally filtered with a low-pass Gaussian filter to reduce high-frequency noise.

Fluorescence traces were normalized by dividing all data points by the average fluorescence at the beginning of each trace before induction of any voltage change. To produce the fluorescence versus voltage graph, $\Delta F/F_o$ was found by taking the average of two regions, one before voltage induction (F_o) and another during voltage induction; the difference between these two averages (ΔF) was then divided by F_o. This value was calculated for each voltage trace and plotted against the membrane potential commanded during voltage induction.

Supporting References

1. Narahashi, T., J.W. Moore, and W.R. Scott. 1964. Tetrodotoxin Blockage of Sodium Conductance Increase in Lobster Giant Axons. J. Gen. Physiol. 47: 965–974.

2. Shapiro, M.G., M.F. Priest, …, F. Bezanilla. 2013. Thermal Mechanisms of Millimeter Wave Stimulation of Excitable Cells. Biophys. J. 104: 2622–2628.

3. Fu, J., J. Gao, …, P. Liu. 2005. An Optimized Protocol for Culture of Cardiomyocyte from Neonatal Rat. Cytotechnology. 49: 109–116.

4. Pusic, A.D., Y.Y. Grinberg, …, R.P. Kraig. 2011. Modeling neural immune signaling of episodic and chronic migraine using spreading depression in vitro. J. Vis. Exp. JoVE. 52.

5. Pusic, A.D., K.M. Pusic, …, R.P. Kraig. 2014. IFNγ-stimulated dendritic cell exosomes as a potential therapeutic for remyelination. J. Neuroimmunol. 266: 12–23.

6. Carlson, G.C., and D.A. Coulter. 2008. In vitro functional imaging in brain slices using fast voltage-sensitive dye imaging combined with whole-cell patch recording. Nat. Protoc. 3: 249–255.